Received: 13 April 2020 | Revised: 15 June 2020 | Accepted: 18 June 2020

DOI: 10.1002/eqe.3316

RESEARCH ARTICLE

WILEY

Evolution of modal characteristics of a mid-rise cold-formed steel building during construction and earthquake testing

Xiang Wang | **Tara C. Hutchinson**

Department of Structural Engineering, University of California, San Diego, La Jolla, California, USA

Correspondence
Tara C. Hutchinson, Department of Structural Engineering, University of California, San Diego, La Jolla, CA 92093-0085, USA.
Email: tara@ucsd.edu

Funding information
U.S. Department of Housing and Urban Development; California Seismic Safety Commission

Summary

Vibration-based structural identification is an essential technique for assessing structural conditions by inferring information from the dynamic characteristics of structures. However, the robustness of such techniques in monitoring the progressive damage of real structures has been validated with only a handful of research efforts, largely due to the paucity of monitoring data recorded from damaged structures. In a recent experimental program, a mid-rise cold-formed steel building was constructed at full scale atop a large shake table and subsequently subjected to a unique multi-hazard scenario including earthquake, post-earthquake fire, and finally post-fire earthquake loading. Complementing the simulated hazard events, low-amplitude vibration tests, including ambient vibrations and white noise base excitation tests, were conducted throughout the construction and the test phases. Using the vibration data collected during the multi-hazard test program, this paper focuses on understanding the modal characteristics of the cold-formed steel building in correlation with the construction and the structural damage progressively induced by the simulated hazard events. The modal parameters of the building (i.e., natural frequencies, damping ratios, and mode shapes) are estimated using two input–output and two output-only time-domain system identification techniques. Agreement between the evolution of modal parameters and the observations of the progression of physical damage demonstrates the effectiveness of the vibration-based system identification techniques for structural condition monitoring and damage assessment.

KEYWORDS

cold-formed steel, damage assessment, modal parameters, shake table tests, system identification

1 | INTRODUCTION

As one of the most widely used nondestructive damage detection techniques, vibration-based structural identification has attracted significant attention amongst civil engineers, as it offers the prospect of assessing the condition and detecting potential damage of structures under extreme events (e.g., earthquakes and hurricanes) or long-term effects (e.g., corrosion and aging).[1,2] These techniques rely on changes in the identified modal parameters (i.e., natural frequencies, damping ratios, and mode shapes) or quantities subsequently derived to detect and localize potential damage of a structure under a routine maintenance plan or following a hazard event since these parameters are correlated

with the change of physical characteristics of the structure (e.g., mass, stiffness, and energy dissipation mechanisms). The modal parameters are often identified from low-amplitude vibration data recorded on the structures, which are considered as equivalent linear viscously damped dynamic systems in the identification procedures. Depending on the availability of input excitation sources, experimental (input–output) and operational (output-only) modal analysis procedures are the main methods used for extracting the modal parameters from recorded vibration data (e.g., other studies[3–5]).

Vibration-based structural identification studies have initially focused on using data simulated by numerical models (e.g., other studies[6–9]) or recorded from small-scale experiments of structural systems and assemblies (e.g., other studies[9–11]). More recently, a large amount of research has been extended to use recorded data obtained from real structures (e.g., buildings and bridges) to monitor their dynamic characteristics under operational conditions (e.g., other studies[12–16]) or during construction and demolition (e.g., other studies[17,18]). However, the monitoring data of real structures do not often involve structural damage induced by extreme loading events (e.g., earthquakes and fire). The limitations of data recorded on structures with real damage have been overcome by recent shake table experiments of large-scale (or full-scale) structures. Such experimental programs have provided unique datasets for understanding the evolution of dynamic characteristics and the damage progression of various structural systems and nonstructural components under extreme loading scenarios (e.g., other studies[19–23]).

Complementing prior large-scale structural experiments, a mid-rise cold-formed steel (CFS) framed building shake table test program was recently conducted to study the seismic and fire performance of such structures.[24–26] This research effort was motivated by the substantial growth in the use of light-frame CFS construction over the past decade or so, particularly in high seismic regions in North America.[27] CFS buildings typically consist of repetitively framed thin-walled steel members (e.g., studs, tracks, and joists) attached with sheathing materials (e.g., gypsum and sheet steel) to form wall-braced structural elements. Their beneficial attributes such as low weight–strength ratio and noncombustibility result in a structural system that is effective in sustaining earthquake and fire hazards. To this end, in the present experimental program, the mid-rise CFS test building was subjected to seven earthquake tests with increased motion intensity before and two earthquake tests after live fire tests conducted on two levels of the building. Complementing the earthquake and fire test sequence, low-amplitude vibration tests, including ambient vibration (AV) and white noise (WN) base excitation tests, were conducted during the construction and earthquake test phases. Vibration test data collected during this earthquake and live fire test program provide a unique opportunity to investigate the effectiveness of structural identification techniques for monitoring progressive structural damage. Utilizing the vibration test data from this experimental program, this paper presents a comprehensive study to understand the evolution of modal parameters of the test building (i.e., natural frequencies, damping ratios, and mode shapes). Importantly, the frequency and story stiffness reductions of the test building estimated using the vibration test data provide quantitative damage metrics for monitoring the conditions of the test building at various stages during the earthquake and fire tests. Agreement between the evolution of the identified modal parameters and the progression of physical damage demonstrates the effectiveness of the vibration-based system identification (SID) techniques for structural damage assessment and health monitoring.

2 | TEST BUILDING

A full-scale CFS wall framed building was designed and constructed on the large high-performance outdoor shake table test facility at UC San Diego (NHERI@UC San Diego).[24–26] The building was assumed to be located in a high seismic region near downtown Los Angeles, with its design basis complying with current code provisions.[28–30] As shown in Figure 1, the test building had a uniform plan dimension of 10.4 × 7.3 m, occupying almost the entire 12.2 × 7.6 m shake table footprint. The total height of the building was 19.2 m above the shake table platen, including a floor-to-floor height of 3.1 m for all six stories and a 1.2 m-tall parapet on the roof perimeter. Consequently, the code-based fundamental period of the test building T was determined as 0.43 s considering a total building height of 18.3 m excluding the parapet. The total weight of the building and its contents was 1160 kN as estimated by averaging the measured vertical loads acting on the shake table during individual earthquake tests.

In terms of layout, the symmetric floor plan consisted of a 1.2-m wide corridor oriented along the longitudinal centerline and a room at each quadrant of the building (Figure 1B). Two transverse partition walls were located 0.6 m west of the transverse centerline (Levels 2 through 6), each separating the two rooms on the same side of the corridor. No partition walls were installed at the first level to retain simplicity in the shake table attachment conditions. To account

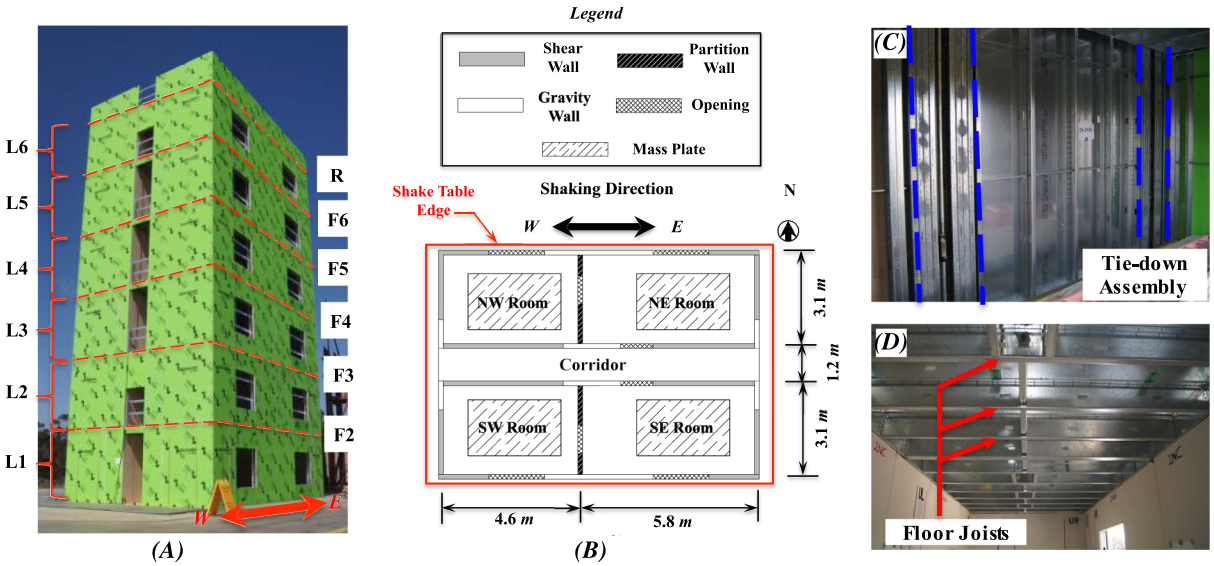

FIGURE 1 Test building: (A) isometric view (arrow denotes shaking direction), (B) building plan layout (typical of Floors 2 to 6), and cold-formed steel structural components: (C) longitudinal corridor shear wall framing, and (D) floor diaphragm framing

for the (seismic) live loads and the weight of certain architectural features excluded from the construction (e.g., flooring and exterior façade finishing), four mass plates were installed on the floor diaphragm at each floor from the second floor through the roof. Each mass plate had a dimension of 3.0 × 1.8 m and a weight of ∼16.5 kN.

The test building was detailed to carry seismic loading using repetitively framed CFS prefabricated wall panels. The primary lateral load resisting system in the direction of shaking (longitudinal axis of the building) consisted of two shear walls placed along each (east and west) end of the corridor, with an associated wall length of 4.0 and 3.3 m for the west and east end walls, respectively. In addition, short shear walls with a length of ∼1.6 m in the longitudinal direction and ∼2.1 m in the transverse direction were placed at the four corners of the building to resist transverse and torsion loads. The shear walls and gravity walls were all fabricated using standard CFS framing members (e.g., studs and tracks). The structural sheathing of the shear walls utilized composite structural panels fabricated using 16-mm thick gypsum boards bonded with a layer of 0.686-mm thick (22 ga.) sheet steel, while the gravity walls were all sheathed with 16-mm thick gypsum boards. In addition, a building tie-down system consisting of steel rods spanning continuously over the entire building height was embedded within the corridor and corner shear walls to provide resistance against building uplift forces (Figure 1C). The floor diaphragms were also constructed using prefabricated CFS-framed panels (Figure 1D). These horizontal structural elements were subsequently connected to the vertical wall systems by attaching the diaphragm joists to the flange of the wall studs via a combination of rim track and clip angle solution (often referred to as the ledger-framed system). The floor sheathing consisted of fiber-reinforced cement boards bonded with a layer of 0.838-mm thick (20 ga.) sheet steel.

3 | EARTHQUAKE AND FIRE TESTS

The three-week test program consisted of a sequence of nine earthquake tests and six live fire tests in three separate test phases. During the pre-fire test phase, the building was subjected to seven earthquake tests with increasing motion intensity levels, namely, serviceability, design, and maximum considered earthquake (MCE) tests. Subsequently, a total of six live fire tests were conducted on the earthquake-damaged building at two select levels (four tests at Level 2 and two at Level 6) across a period of three consecutive days. The test program concluded with two post-fire earthquake tests (serviceability followed by MCE) on the final test day. It is noted that all the earthquake test motions were applied in the east–west direction using the single-axis shake table, whose axis coincided with the longitudinal axis of the building. In addition, the physical damage of the structural system induced by the earthquake and fire tests was inspected and documented at six critical stages throughout the test program: (a) beginning of the test phase (before EQ 1), (b) following the service level test sequence EQ 1–EQ 3, (c) following the design event test EQ 6, (d) end of the pre-fire

earthquake test phase (following EQ 7), (e) end of the fire test phase, and (f) end of the post-fire earthquake test phase (following EQ 9).

Table 1 summarizes the peak building responses associated with individual earthquake tests, whereas the story shear versus interstory drift ratio (IDR) hysteresis response at select earthquake tests are shown in Figure 2. It is noted that the seismic drift demands, such as peak IDR (PIDRs) and peak roof drift ratios (PRDRs), serve as important proxies for assessing the structural damage of the building. In addition, examples of representative physical damage to the building occurred during the earthquake and fire test sequence are illustrated in Figure 3. The key response and the observed damage of the test building at the various stages of the test sequence are summarized as the following:

- *Pre-fire serviceability level earthquake tests (EQ 1–EQ 4)*: Drift demands of the building were relatively low (PIDR <0.1%). The building response remained essentially linear (Figure 2 left); the structure sustained only limited instances of minor damage (e.g., incipient screw withdrawal and wall sheathing panel crushing at the corner or edge).
- *Pre-fire design level (EQ 6) and MCE (EQ 7) earthquake tests*: As drift demands increased substantially (~1.0% in the design event and >1.5% in the MCE event), the building response became highly nonlinear (Figure 2 middle and right). Damage to the sheathing panels of the corridor walls became pervasive at all but the uppermost levels. Typical

TABLE 1 Summary of the test sequence and the associated peak building responses

Earthquake test date	Test motion	Performance target	PFA (g) (floor #)	PIDR (%) (level #)	PRDR (%)	RDR_{res} (%)
Day 1 (13 June 2016)	EQ 1: RIO-25	Serviceability	0.35 (R)	0.08 (L4)	0.05	0.0
	EQ 2: CNP-25		0.38 (R)	0.09 (L4)	0.07	0.0
	EQ 3: CUR-25		0.45 (R)	0.10 (L4)	0.08	0.0
Day 2 (15 June 2016)	EQ 4: CNP-25		0.43 (R)	0.10 (L4)	0.09	0.0
	EQ 5: CNP-50	50% Design	0.85 (R)	0.24 (L3)	0.19	0.0
	EQ 6: CNP-100	Design	2.07 (R)	0.89 (L4)	0.70	0.0
Day 3 (17 June 2016)	EQ 7: CNP-150	MCE	3.77 (F5)	1.70 (L4)	1.49	0.1
Fire test sequence (27–29 June 2016)						
Day 4 (1 July 2016)	EQ 8: RIO-25	Serviceability	0.16 (R)	0.17 (L3)	0.12	0.0
	EQ 9: RRS-150	MCE	4.43 (F5)	12.15 (L2)	2.84	1.2

Abbreviations: PFA, peak floor acceleration; PIDR, peak interstory drift ratio; PRDR, peak roof drift ratio; RDR_{res}, residual roof drift ratio (within an individual test); MCE, maximum considered earthquake.

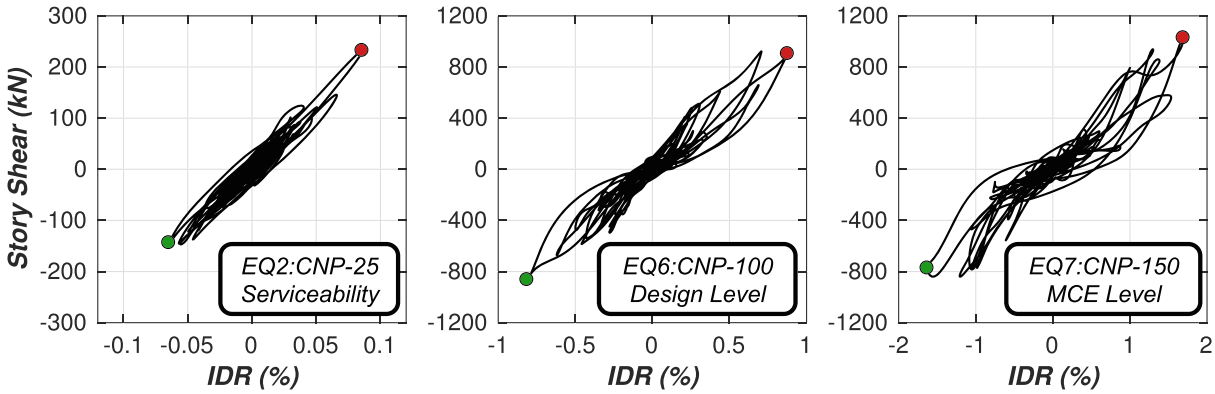

FIGURE 2 Story shear versus interstory drift ratio (IDR) response at Level 4 during three select earthquake tests. MCE, maximum considered earthquake

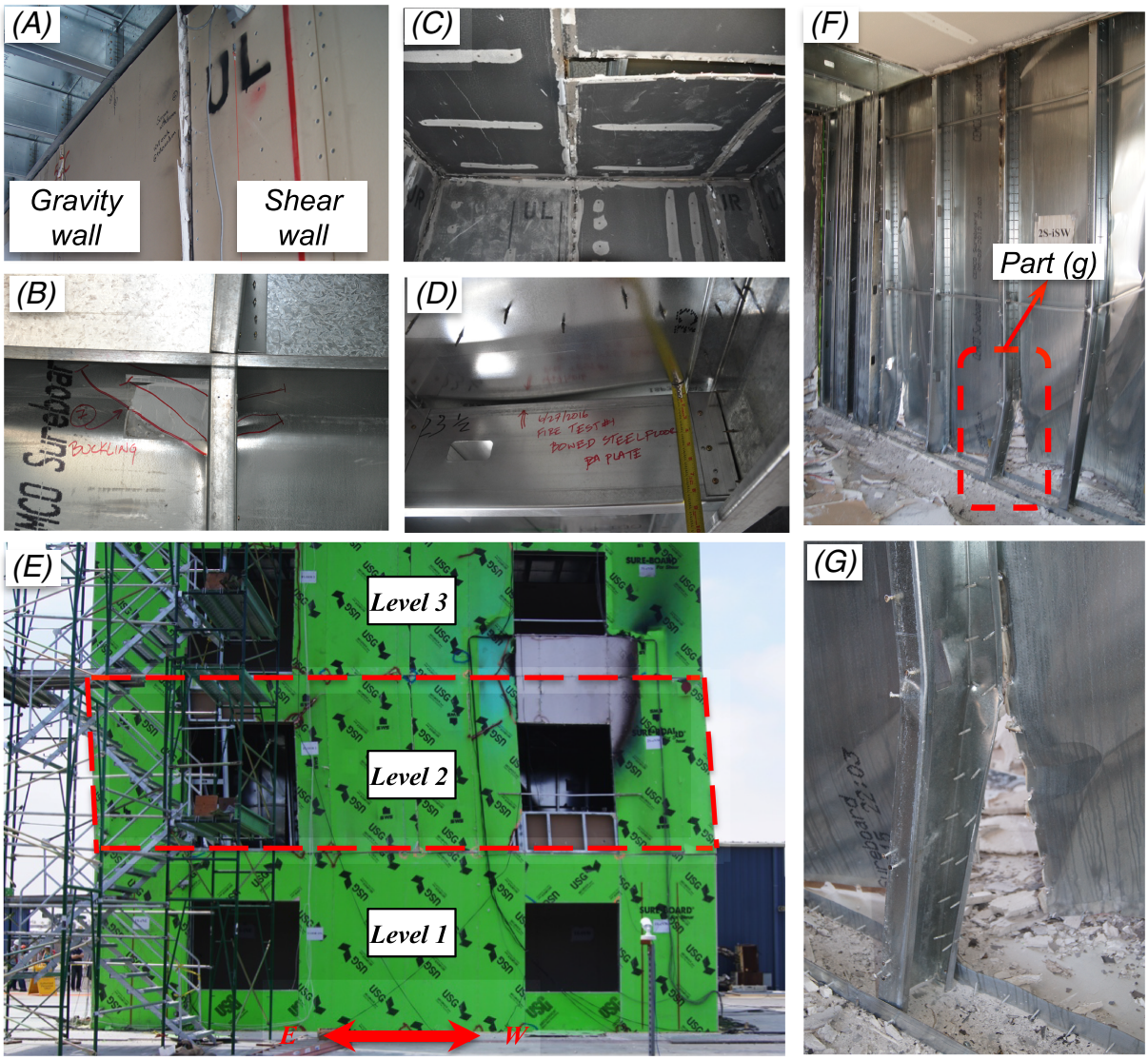

FIGURE 3 Physical damage of test building: (A) gravity wall and shear wall boundary gypsum crushing (moderate damage, after EQ 7), (B) structural panel sheathing steel sheet buckling (moderate damage, after EQ 7), (C) detached ceiling gypsum panel (after fire test), (D) floor diaphragm sagging (after fire test), (E) soft story mechanism at Level 2 (severe damage, after EQ 9), (F) Level 2 corridor shear wall with detached structural panels and buckled steel framing (severe damage, after EQ 9), and (G) zoom-in view of structural panel detachment and steel stud buckling (severe damage, after EQ 9)

damage included significant crushing along the shear wall and gravity wall boundaries (Figure 3A) and buckled sheet steel of the corridor shear wall sheathing (Figure 3B). It is noted, however, that damage that occurred during the pre-fire earthquake test phase was characterized as moderate since the damaged sheathing remained repairable or readily replaceable.

- *Fire tests*: Room temperature exceeded 1000°C in four out of six live fire tests, resulting in loss of strength and rigidity for the wall and floor sheathing panels. Fire-induced damage occurred in the form of partially detached ceiling gypsum boards (Figure 3C) and large deflection of the floor diaphragm at the second floor (Figure 3D).
- *Post-fire MCE earthquake test (EQ 9)*: The building sustained excessively large drift demands (PIDR >12% at Level 2 and 1.2% residual roof drift ratio [RDR]), resulting in a soft-story mechanism at Level 2 and a near-collapse condition (Figure 3E). The structural walls at Level 2 suffered extremely severe damage in the form of complete detachment of shear wall structural panels as well as global and local buckling of the framing members (studs and tracks) (Figure 3F,G). Despite the excessive damage (particularly at Level 2), the building resisted collapse largely due to the presence of the building tie-down system, which facilitated framing action and subsequent redistribution of lateral earthquake loads.[26]

4 | LOW-AMPLITUDE VIBRATION TESTS

A sequence of low-amplitude vibration tests was performed throughout the construction and test phases to allow for a systematic study of the evolution of modal characteristics of the test building. The vibration tests involved white noise (WN) base excitation tests in the construction and test phases as well as ambient vibration (AV) tests in the test phase. The amplitude of WN tests, measured in terms of the root-mean-square (RMS) acceleration of the target base excitation, was selected as either 1.5% *g* RMS or 3.0% *g* RMS (hereafter, referred to as 1.5% *g* or 3.0% *g* WN tests for brevity). All the WN tests were conducted with a duration of 180 seconds. In contrast, the duration of the AV tests was much longer than those of the WN tests, with typical data durations of 1200–1440 seconds. Interested readers are referred to Wang et al.[25] for additional details of the low-amplitude vibration tests.

4.1 | Vibration test sequence

Figure 4 illustrates the timeline of the low-amplitude vibration test sequence throughout the construction and test phases. Following the completion of the structural skeleton erection, WN tests were performed at five different stages, namely denoted as C1–C5, during the construction phase. The different stages were characterized by varied roof mass plate layouts and interior construction aspects (e.g., attachment condition of the interior gypsum wall panels and partition wall installation). Since the primary goal of these WN tests was to explore the impact of interior gypsum and partition wall installation on the dynamic characteristics of the test building, the study focuses on the last three states during the construction phase, namely, C3–C5. State C3 represented the test building following the structural skeleton erection with minimally attached interior gypsum and partition wall framing installed. In contrast, States C4 and C5 represented essentially identical states at the completion of all construction activities with fully attached interior gypsum and completed partition walls. The test building remained in the same condition between the completion of construction activities and the beginning of the test phase, therefore, States C4 and C5 were considered equivalent with the reference (initial) State S0 during the test phase (see discussions in the next paragraph).

A total of 11 states (S0–S10) are defined over the test phase timeline, each corresponding to a specific damage condition of the test building. In addition, the availability of the low-amplitude vibration data recorded by different data monitoring systems at each state is annotated by different symbols (see detailed discussions in the following section). State S0 is defined as the reference state for comparing the evolution of the modal parameters at all subsequent states (i.e., S1 through S10). It is noted that States S3 and S6 appear twice on different test dates because no damage occurred between the end of one test date and the beginning of the following test date. The WN tests were conducted before and after each earthquake test except at State S10 due to the severity of building damage (see Figure 3E–G). In contrast, the

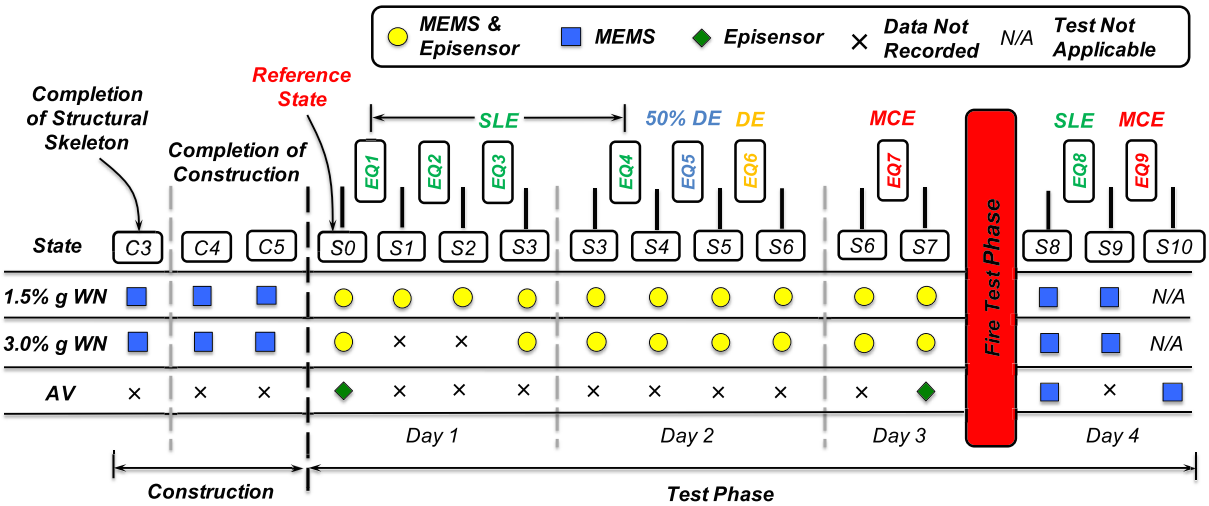

FIGURE 4 Timeline of low-amplitude vibration test protocol during construction and test phases

AV tests occurred at only four key stages throughout the test phase, namely, the beginning and the end of the pre-fire (States S1 and S7) as well as the post-fire earthquake test phase (States S8 and S10).

4.2 | Instrumentation

The floor accelerations of the building were measured by two separate monitoring systems: (a) a dense array of uniaxial micro-electro-mechanical system (MEMS) accelerometers sampling data at a frequency of 240 Hz (Figure 5A) and (b) a relatively sparse array of uniaxial Episensor force balance accelerometers sampling data at a frequency of 200 Hz (Figure 5B). It is noted that the MEMS accelerometers offer the frequency and amplitude range for capturing anticipated building response during the earthquake and WN tests, whereas the Episensor system was added to this test program due to their low noise floor and high dynamic range, thus improving the potential to collect robust AV data. The MEMS accelerometers were distributed at the four corners at all floors as well as the table platen (the first floor), although the sensor numbers varied between 25 accelerometers at the beginning of the construction phase and 68 accelerometers during the earthquake test phases. In contrast, the Episensor system consisted of three accelerometers (two in the longitudinal direction and one in the transverse direction) at each of four select floors (Floors 2, 4, 6 and roof) excluding the table platen, resulting in 12 accelerometers in total. It was deployed to the building only at the pre-fire earthquake test phase. Additional details regarding the instrumentation plans of the two accelerometer arrays are available in Wang et al.[25]

As shown in Figure 4, WN data were collected by the MEMS system at all states during the construction phase as well as all except the last states (S0–S9) during the test phase. The Episensor system also collected WN data at the pre-fire earthquake test phase (S0–S7); however, no accelerometers were installed on the table platen to record the WN base excitations. As a result, WN data collected by the MEMS system are considered as the primary dataset due to its completeness availability of WN input excitations and consistency (i.e., availability throughout the construction and test phases). In addition, AV data were collected by the Episensor system during the pre-fire earthquake test phase (States S1 and S7) and by the MEMS system during the post-fire earthquake test phase (States S8 and S10). Importantly, the AV data collected at State S10 provide the only dataset for identifying the modal characteristics of the building at its final state, since conducting WN base excitation tests at this state was deemed unsafe due to the severity of damage sustained by the building (Figure 3E–G).

4.3 | Building acceleration response

To demonstrate the time- and frequency-domain characteristics of the low-amplitude vibration data, Figure 6 compares the roof acceleration time histories of the building recorded during the WN and AV tests at the reference state (S0) as well as the associated power spectral density (PSD). The PSD is estimated using Welch's method,[31] in which the acceleration is divided into 20 equal segments with a 50% overlap. Because the WN base excitation was applied along the longitudinal axis of the building, the amplitude of the transverse acceleration was significantly smaller than its longitudinal counterpart (as low as 5% as shown in Figure 6A). The lack of comparable amplitudes of the building response during the WN tests resulted in very low modal participation of the building transverse vibration and tends to pose difficulties for identifying the transverse modes. The PSD indicates that the dominated spectral peaks of both the longitudinal and

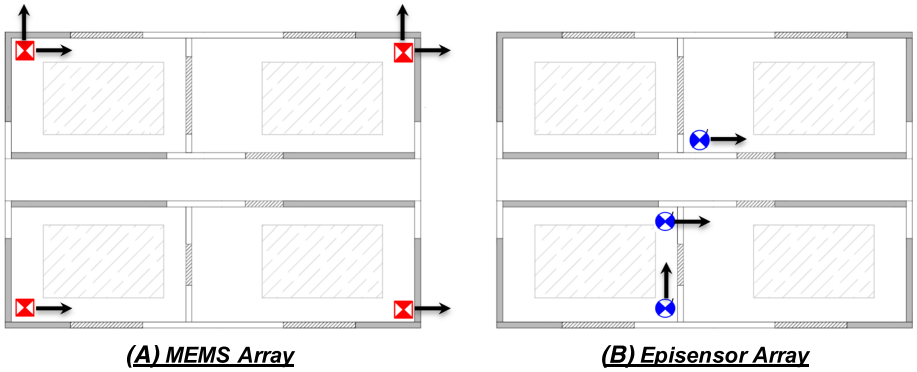

FIGURE 5 Accelerometer plan layout: (A) *MEMS array* (typical of all floors including roof) and (B) *Episensor array* (typical of Floors 2, 4, 6 and roof). Note that the arrow direction denotes sensor orientation. Micro-electro-mechanical system (MEMS) [Colour figure can be viewed at wileyonlinelibrary.com]

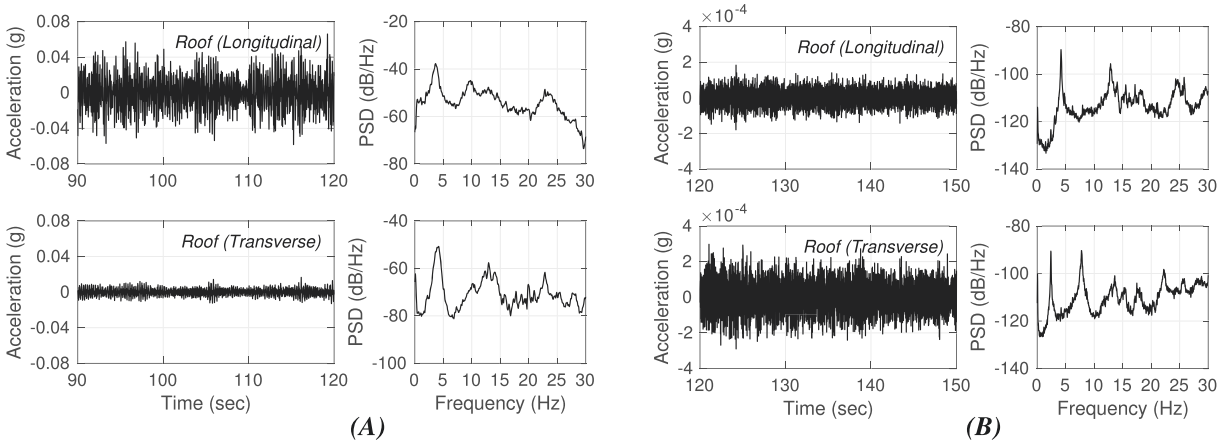

FIGURE 6 Roof acceleration time histories and the associated power spectral densities (PSDs) at the reference state (S0): (A) 1.5% *g* white noise (WN) test (recorded by *MEMS*) and (B) ambient vibration (AV) test (recorded by *Episensor system*). Note: MEMS = micro-electro-mechanical system

transverse responses were associated with the longitudinal and torsional vibration of the building, while the transverse vibration modes are barely identifiable.

The acceleration responses of the building during the AV test (Figure 6B) differed from those of the WN test in several aspects: (a) smaller amplitude in both the longitudinal and transverse directions (about two orders of magnitude lower than the longitudinal building responses during the WN tests), (b) comparable amplitude in the two directions, and (c) longer duration of the recorded data (10 min or longer for AV tests compared with 3 min for WN tests). Due to the proportionate amplitudes of acceleration responses in the longitudinal and transverse directions, the building vibration modes in the two directions were both observable from the spectra. In addition, the PSD estimated using the AV data are characterized by sharper spectral peaks compared to those of the WN tests, indicating smaller damping ratios for these vibration modes during the AV tests.

5 | SID RESULTS

5.1 | Methods and procedures

In the system identification (SID) study, the modal parameters (i.e., natural frequencies, damping ratios, and mode shapes) of the test building during the low-amplitude vibration tests are analyzed using two input–output SID methods, (a) deterministic-stochastic subspace identification (DSI) method[32] and (b) observer/Kalman filter identification combined with Eigensystem realization algorithm (OKID-ERA) method,[33,34] as well as two output-only methods, (c) data-driven stochastic subspace identification (SSI-DATA) method,[32,35] and (d) multiple-reference natural excitation technique combined with Eigensystem realization algorithm (NExT-ERA) method.[36] Each of these time-domain SID methods considers the test building as a linear time-invariant state-space model, in which all sources of energy dissipation are represented by linear viscous damping. In addition, these methods assume the excitation sources of the vibration tests to be broadband stationary excitations. The use of different SID methods provides intramethod and intermethod comparisons to evaluate the consistency of the estimated modal parameters as well as the robustness of these methods when their underlying assumptions are not strictly satisfied (e.g., linear time-invariant system, broadband excitation, and stationary response). These methods have been successfully implemented in the SID studies of large-scale structures in previous shake table experiments (e.g., other studies[19–23]). Discussion of the theoretical background and implementation details of these SID methods is outside of the scope of this paper. Interested readers are referred to relevant literature for a comprehensive review of the SID methods.

The use of input–output or output-only methods depends on the type of vibration tests as well as data collected by the specific monitoring system. The output-only methods are used in conjunction with all AV data and WN data collected by the Episensor system because the system input was either unknown or not recorded in these tests. In contrast, the input–output methods are used in conjunction with WN data collected by the MEMS. Specifically, the

system input is taken as the averaged longitudinal acceleration of the table platen, whereas the system output involves two longitudinal accelerations (northwest and southwest corners) and two transverse accelerations (northwest and northeast corners) at all floors of the building from the second floor to the roof, resulting in a total of 24 output channels. In the data preprocessing procedures, the raw acceleration response recorded by each channel is first decimated to 80 Hz to reduce the computational costs and subsequently filtered using a fourth order band-pass Butterworth filter (with cut-off frequencies at 0.25 and 25 Hz). It is noted that the Nyquist frequency of the processed data of 40 Hz remains sufficiently large to involve all the vibration modes that contribute noticeably to the building response.

To distinguish structural modes from spurious (mathematical) modes in the SID results, stability diagrams are employed to examine the consistency of identified modal parameters over a consecutive sequence of model orders.[37] In this study, the stability thresholds of the identified modal parameters (i.e., frequency, damping ratio, and modal assurance criterion [MAC][38]) are defined as the following:

$$\left|\frac{f_i - f_{i+1}}{f_{i+1}}\right| \le 0.02, \quad \left|\frac{\xi_i - \xi_{i+1}}{\xi_{i+1}}\right| \le 0.05, \quad 1 - \mathrm{MAC}\left(\phi_i, \phi_{i+1}\right) \le 0.02, \tag{1}$$

where f_i, f_{i+1}, ξ_i, and ξ_{i+1} are the natural frequencies and damping ratios identified from two consecutive model orders, MAC (ϕ_i, ϕ_{i+1}) is the modal assurance criterion of a pair of mode shape vectors at two consecutive model orders. The identified modes are considered as stable when the triple convergence criteria (frequency, damping ratio, and MAC) are satisfied for at least six consecutive model orders (note that the model order increases with an increment of two).[37]

5.2 | Modal parameters identified from WN tests

Using WN data collected by the MEMS, the modal parameters of the building are identified by the input–output (DSI and OKID-ERA) and output-only methods (SSI-DATA and NExT-ERA). Figure 7 illustrate the mode shapes of the six stable modes and the corresponding polar plot representations of the complex-valued mode shapes identified from the 1.5% *g* WN test at State S0 (reference state) by the DSI (input–output) method. Absent substantial stiffness and mass irregularities for the test building, the first three identified modes correspond to the first transverse (1-T), longitudinal (1-L), and torsional (1-To) vibration modes, whereas the last three identified modes correspond to the second transverse (2-T), longitudinal (2-L), and torsional (2-To) vibration modes. In addition, the polar plots indicate that all the identified modes are nearly classically damped because the mode shape components are nearly collinear. However, the stability

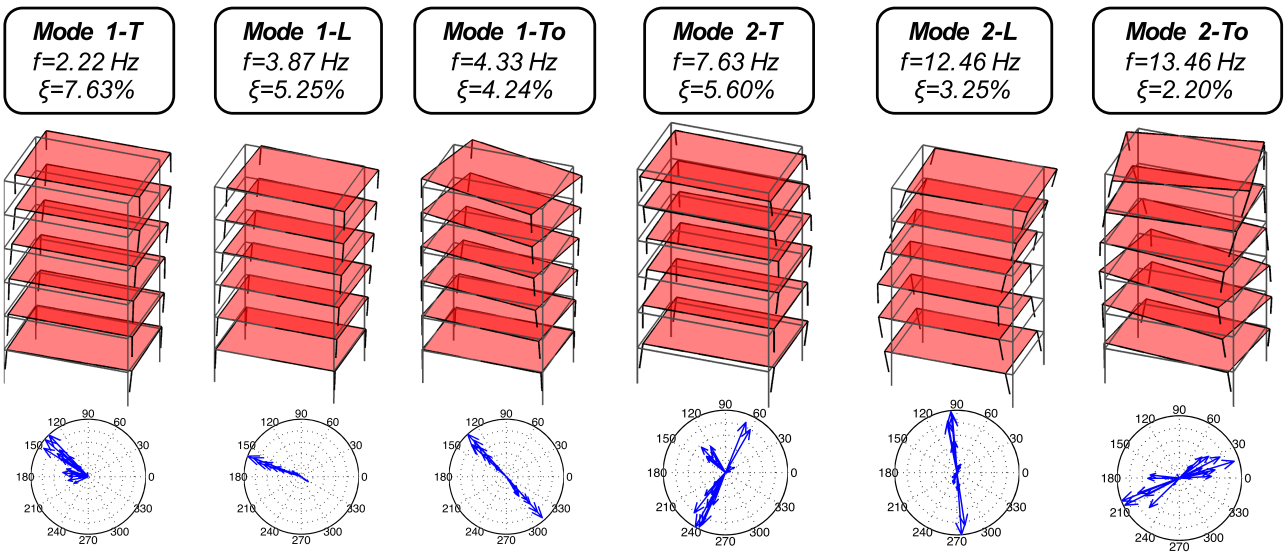

FIGURE 7 Mode shapes and the corresponding polar plot representation of the mode shape vectors obtained from the 1.5% *g* white noise (WN) test at State S0 (reference state) using the deterministic-stochastic subspace identification (DSI) method [Colour figure can be viewed at wileyonlinelibrary.com]

thresholds are more difficult to satisfy for the transverse modes (1-T and 2-T) since the transverse vibration of the building may not be sufficiently excited during the WN tests due to the much lower amplitude of input excitations in this direction.

To validate the effectiveness of the SID results, Figure 8 compares the measured longitudinal floor accelerations of three select floors (i.e., Floors 2 and 4 and roof) with the corresponding responses simulated using the state-space models identified from the 1.5% *g* WN tests at three select states (S0, S7, and S8). The relative RMS error (RRMSE) between the measured and simulated responses are also summarized in the plots to provide error metrics for assessing the SID results. The RRMSE is defined herein as the RMS of the error between the measured and simulated responses normalized by the RMS of the measured response. Agreement between the measured and simulated acceleration responses (~12% RRMSE) at the reference state (S0) demonstrates that the identified state-space models accurately replicate the dynamic responses of the test building under its initial (undamaged) condition. As a result of the building damage progression at States S7 (end of pre-fire test phase) and S8 (beginning of post-fire test phase), the discrepancies between the measured and simulated responses become noticeably larger (~20% RRMSE). The increase in the errors implies that a linear time-invariant model may reduce the accuracy of the state-space model for characterizing the dynamic responses of the damaged building. Nevertheless, this error level is considered reasonable given the severity of building damage at these two states (S7 and S8).

5.2.1 | Construction phase—WN tests

Figure 9 summarizes the natural frequencies of the building at three select states during the construction phase (C3–C5) as identified from the WN data. The corresponding damping ratios are presented in Figure 10. As mentioned earlier, State C3 represented the building with minimally attached interior gypsum and partially installed partition wall framing, whereas States C4 and C5 represented essentially identical states at the completion of all construction activities when all interior gypsum panels were fully attached to the structural wall framing and partition wall installation was complete. The results include the modal parameters of the longitudinal (1-L and 2-L) and torsional (1-To and 2-To) modes, whereas the transverse modes (1-T and 2-T) do not consistently meet the stability thresholds due to the disparity in amplitudes between the longitudinal and transverse WN excitations. To evaluate the performance of individual SID methods and demonstrate the method-to-method variability of the results, these figures compare the modal parameters

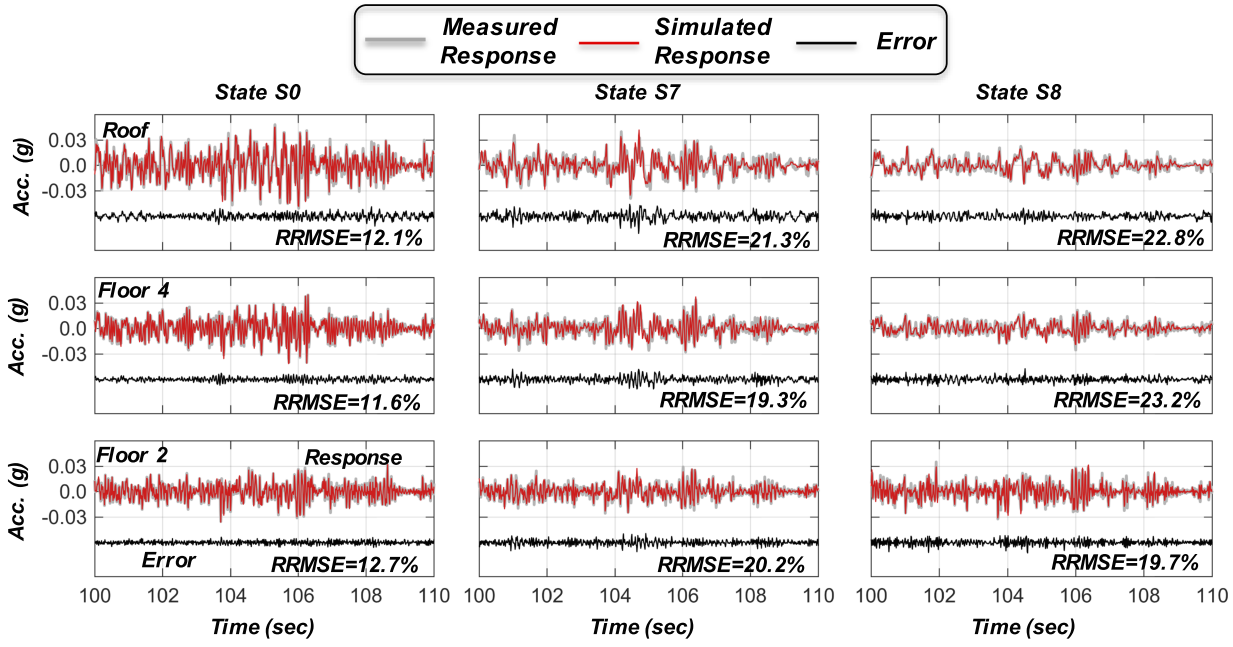

FIGURE 8 Comparison of measured and simulated longitudinal floor accelerations during the 1.5% *g* white noise (WN) tests at three select states: S0 (reference state, beginning of pre-fire test phase), S7 (end of pre-fire test phase), and S8 (beginning of post-fire test phase). Note that RRMSE denotes relative root-mean-square error

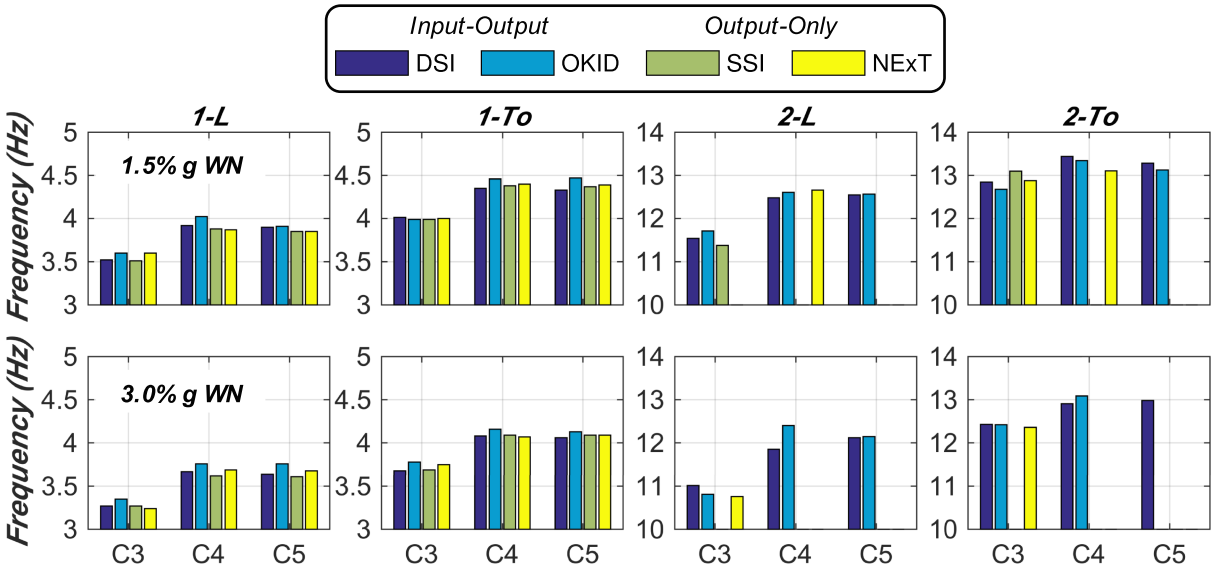

FIGURE 9 Natural frequencies identified from the white noise data during the construction phase using four system identification methods. DSI, deterministic-stochastic subspace identification; NExT, natural excitation technique; OKID, observer/Kalman filter identification; SSI, stochastic subspace identification

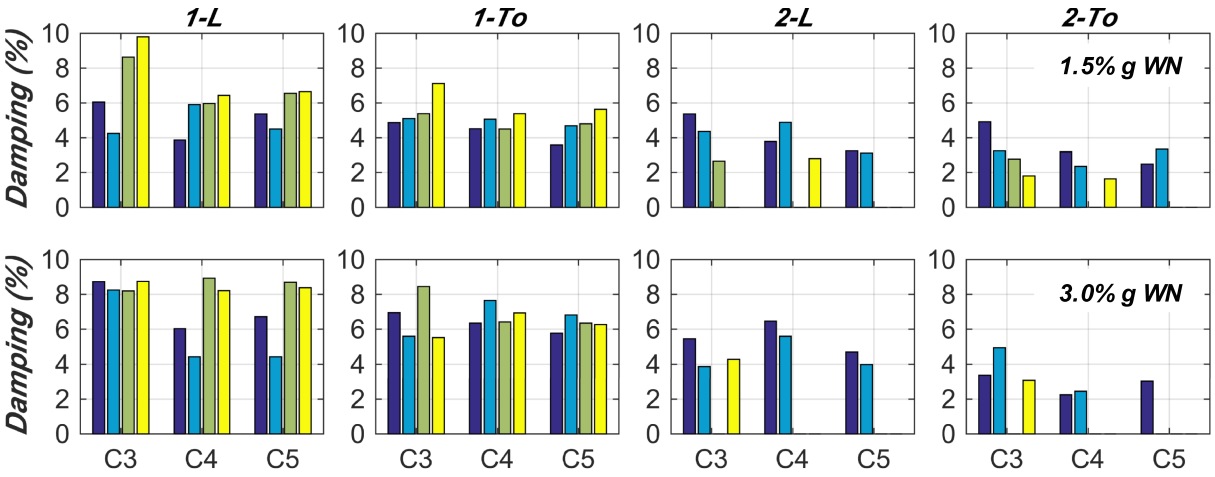

FIGURE 10 Damping ratios identified from the white noise (WN) data during the construction phase using four system identification methods

identified using both the input–output (DSI and OKID-ERA) and output-only (SSI-DATA and NExT-ERA) methods. In terms of the performance of different methods, all of the input–output and output-only methods are capable of identifying the fundamental modes of the test building (1-L and 1-To). However, the output-only methods are outperformed by the input–output methods in the higher mode identification (2-L and 2-To). This is attributed to the fact the achieved test excitations contained a salient spectral peak at around 10 Hz due to the oil column resonance effect of the shake table hydraulic system,[25] while the spectral density of input excitations are assumed to be constant in the output-only methods. Since oil column resonance effects are ubiquitous for hydraulic-mechanical shake table systems, neglecting the resonance effect particularly undermines the capacity of the output-only methods in capturing the vibration modes (2-L and 2-To) whose frequencies (11–13 Hz) fall into the oil resonance frequency region (∼10 Hz). Comparisons of the modal results identified using different SID methods reveal that the natural frequencies are in reasonable agreement at all three states (Figure 9). The frequency errors of less than 3% amongst the four different methods demonstrate the consistency of identified modal frequencies. In contrast, the damping ratios are subjected to much larger method-to-method variations (Figure 10). The differences between the damping ratios identified using the two input–output

methods differ by as much as 25%–30% (with respect to the average value). The distinctions amongst the identified damping ratios become even greater amongst the input–output and output-only results. The method-to-method variability of identified damping ratios is consistent with the findings from prior large-scale structure shake table experiments (e.g., other studies[19,23]).

Since the input–output methods appear more effective in the higher mode identification, the evolution of modal parameters during the construction phase are discussed based on the results identified using the input–output methods. The natural frequencies of the two longitudinal modes (3.7 Hz for Mode 1-L and 13.0 Hz for Mode 2-L during the 3.0% *g* WN tests) at States C4 and C5 were roughly 10% higher than those at State C3 (3.3 Hz for Mode 1-L and 12.4 Hz for Mode 2-L during the 3.0% *g* WN tests). The increase of the natural frequencies is indicative of the stiffness contribution from the fasteners that attached the interior gypsum panels to the CFS framing and the partition walls. In contrast, the differences in the damping ratio between States C4 (or C5) and C3 do not reveal a consistent trend between the building interior installation and the damping ratios. Besides, the natural frequencies and damping ratios appear to be dependent on the amplitudes of the WN excitations. As the WN amplitude increases from 1.5% *g* to 3.0% *g*, the natural frequencies of all identified modes undergo a consistent reduction of 5%–10%, while the damping ratios of Modes 1-L and 2-L rise by 20%–30%.

5.2.2 | Test phase—WN tests

The WN tests conducted during the earthquake test phase allowed for investigating the evolution of modal parameters of the building in correlation with the progression of physical damage of the test building. For brevity, discussions of the modal parameters herein focus on results identified using the DSI (input–output) method. The modal parameters identified using the other three SID methods are available in Wang et al.[25] Figure 11 presents the modal parameters of the longitudinal (1-L and 2-L) and torsional (1-To and 2-To) modes identified from the test phase WN data. This figure shows that the progression of physical damage reduces the natural frequencies and increases the damping ratios for all four identified modes (i.e., 1-L, 1-To, 2-L, and 2-To). The modal parameters of all the identified modes remained nearly constant during the serviceability level test sequence (States S0–S4). Reduction of the natural frequencies initiated at State S5 (following EQ 5: 50% design event) and became more pronounced at State S6 (following EQ 6: design event) and S7 (following EQ 7: MCE event). Since the longitudinal shear walls (in parallel with the shaking direction) suffered much more severe damage than that of the transverse walls, the natural frequencies of the longitudinal modes (1-L and 2-L) reduced more significantly than those of the torsional modes (1-To and 2-To). In addition, the damping ratios of all the identified modes increased sharply at States S5 and S6 and remained stable at State S7. Following the pre-fire test sequence, the identified modal parameters remained essentially stable over the last three States (S7–S9), indicating that the fire tests and the post-fire serviceability earthquake test (EQ 8) did not induce substantial damage to the building. As opposed to the natural frequencies and damping ratios, the mode shapes appear less sensitive to the physical damage because the MAC values (between the reference state and subsequent states) of the longitudinal modes (1-L and 2-L) remained sufficiently close to unity (>0.95) throughout the test sequence, although they reduce slightly (but remained >0.9) for the torsional modes (1-To and 2-To).

Consistent with those observed from the construction phase WN data, the natural frequencies and damping ratios are also found to be dependent on the amplitude of the WN excitations. At all 10 states (S0–S9) during the test phase, increasing the WN amplitude from 1.5% *g* to 3.0% *g* consistently reduces the natural frequencies (about 10%) and increases the damping ratios (typically 20%–30% but exceeded 50% in several cases). In addition, the damping ratios of the fundamental modes (1-L and 1-To) appear larger than those of their respective higher modes (2-L and 2-To). During the serviceability level test sequence (States S0–S4), the identified damping ratios exceeded 5% for the first longitudinal mode (1-L), as opposed to only about 3% for the second longitudinal mode (2-L).

To further demonstrate the effect of damage progression on the modal characteristics of the test building, Figure 12 illustrates the frequency response functions (FRFs) between the longitudinal roof (output) and table platen (input) accelerations under the WN tests at four select states (S0, S3, S6, and S7) during the pre-fire test phase. The FRF is estimated as the quotient of the cross PSD of the input and output over the auto PSD of the input. Since the building sustained only limited damage (<0.1% PRDR) at the serviceability level test sequence (State S3), the FRF contained three distinct spectral peaks associated with the first three longitudinal vibration modes. The progression of structural damage during the design level (EQ 6 with a PRDR of 0.7%) and MCE level (EQ 7 with a PRDR of 1.5%) tests resulted in remarkable frequency shift (reduction) of the spectral peaks as well as smaller magnitude and broader bandwidth for

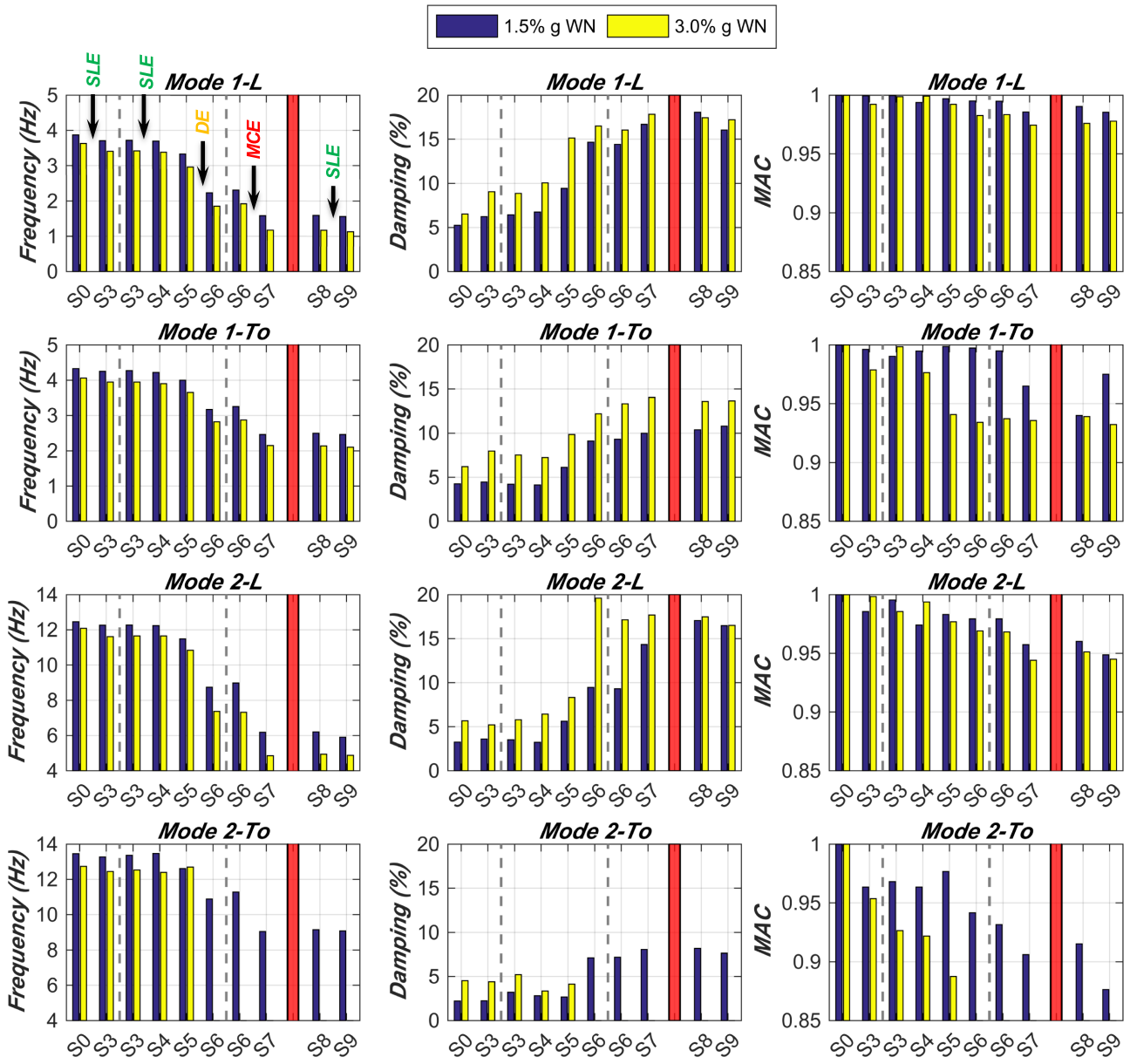

FIGURE 11 Modal parameters identified from the white noise (WN) data during the test phase (dashed vertical lines divide earthquake test dates; vertical red bar denotes the fire test phase; DE, design level; MAC, modal assurance criterion; MCE, maximum considered earthquake ; SLE, serviceability)

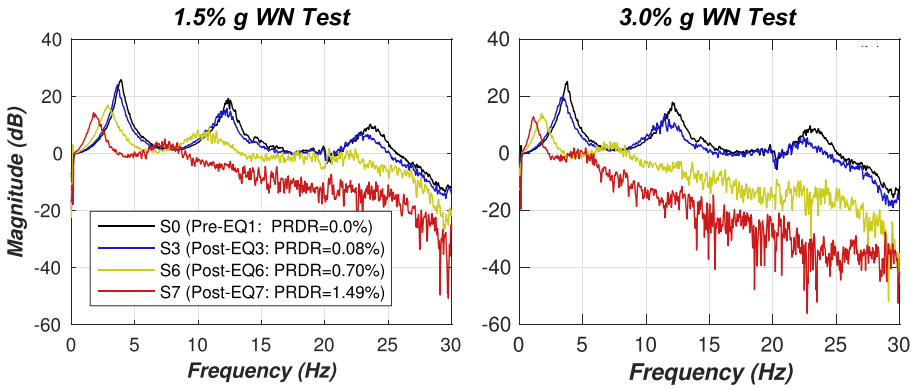

FIGURE 12 Frequency response functions under the white noise (WN) tests at four select states of the test phase (refer to Figure 4 for test sequence). PRDR, peak roof drift ratio

these peaks (indicative of increased damping ratios). For the 1.5% *g* WN tests, the spectral peak of the first longitudinal mode shifted from ~4 Hz at State S0 to less than 2 Hz at State S7, while its magnitude decreased from ~25 dB at State S0 to ~15 dB at State S7. Importantly, the spectral peaks of the higher modes became less identifiable at States S6 and S7 due to the progression of structural damage.

5.3 | Modal parameters identified from AV tests

AV test data were collected at four key stages during the test phase, namely, the beginning and end of both pre-fire and post-fire test phases, namely, S1, S7, S8, and S10 (also refer to Figure 4 for test sequence). Importantly, the AV data allow for assessing the dynamic characteristics of the building at the final state (S10) when the building sustained extreme damage (see Figure 3E–G). Besides, the transverse vibration modes of the test buildings are consistently identified using the AV data due to the commensurate excitation amplitudes in the two horizontal directions. Note that AV data were collected using only the Episensor system at the pre-fire test phase (States S1 and S7) and only the MEMS system at the post-fire test phase (States S8 and S10). Since the first transverse and longitudinal (1-T and 1-L) modes are the only two stable modes associated with the final state (S10), result discussions herein focus on the modal characteristics of these two vibration modes.

The modal parameters of the building are identified using the two output-only methods (SSI-DATA and NExT-ERA) due to the unknown input excitations of the AV tests. Figure 13 presents the identified natural frequencies and damping ratios of the first transverse and longitudinal modes (1-T and 1-L) at all four states. Notably, the agreement between both the natural frequencies and damping ratios identified using the two methods verifies the effectiveness of

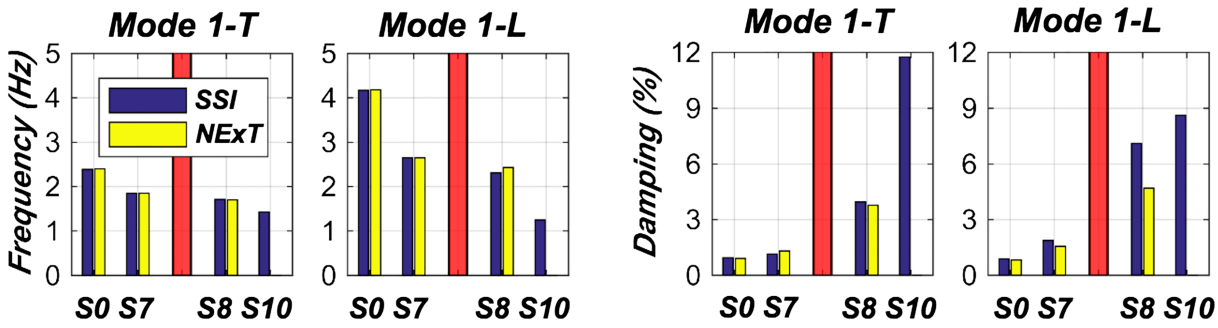

FIGURE 13 Natural frequencies and damping ratios identified from the ambient vibration (AV) data during the test phase (vertical red bar denotes the fire test phase)

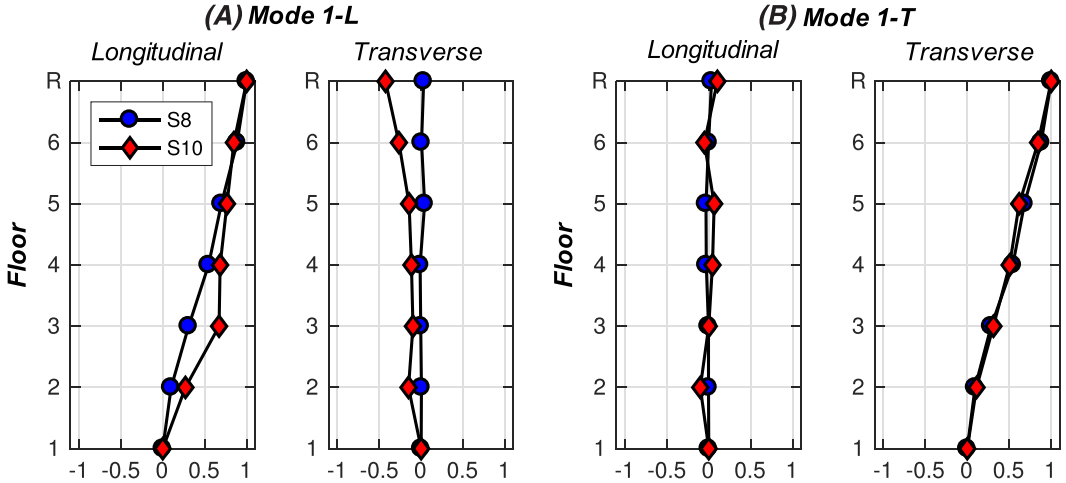

FIGURE 14 Comparison of the mode shape components of (A) Mode 1-L and (B) Mode 1-T between the beginning (S8) and end of the post-fire test phase (S10)

the methods. Compared with that at the reference state (S0), the natural frequency of the first longitudinal mode (1-L) reduced by 40% at the end of the pre-fire test phase (State S7) and dropped only another 10% following the fire tests (State S8), whereas the frequency reduction of the first transverse mode (1-T) was much smaller at the corresponding state (∼25% reduction from S0 to S8). The final earthquake test resulted in a drastic frequency reduction for Mode 1-L (from 2.3 Hz at State S8 to 1.25 Hz at State S10), whereas the frequency of Mode 1-T decreased by only ∼15% (from 1.71 Hz at State S8 to 1.43 Hz at State S10). Figure 14 compares the mode shape components of Modes 1-L and 1-T at the beginning and end of the post-fire test phase (States S8 and S10). While the mode shape of Mode 1-T remained consistent between States S8 and S10 (with a MAC value of 0.98), the mode shape of Mode 1-T at State S10 differed significantly from that at State S8 (with a MAC value of 0.85). Particularly, the mode shape of Mode 1-L was characterized by nonproportionally large deflection concentrated at Level 2 in the longitudinal direction as well as large-amplitude transverse deflection (∼50% the longitudinal counterpart at the roof level) at the final state (S10). This remarkable difference of the first longitudinal mode clearly reveals the formation of soft story mechanism at Level 2 at the end of post-fire test phase, see Figure 3E.

6 | DAMAGE ASSESSMENT VIA FREQUENCY AND STORY STIFFNESS REDUCTIONS

6.1 | Frequency reduction

Since the natural frequencies identified using different SID methods tend to be more consistent than the damping ratios, frequency reduction is adopted as a global damage metric to quantitatively assess the progression of the building damage during the test program. The damage assessment herein focuses only on the first and second longitudinal vibration modes (1-L and 2-L) because the structural walls oriented in this direction (in parallel with the shaking direction) were subjected to in-plane earthquake excitations and thus sustained much more severe damage than that of the transverse walls. In this study, the frequency reduction of a specific vibration mode is a percentage defined as the frequency difference between the subsequent state (i.e., S3 through S9) and the reference state (S0) normalized by the frequency of the reference state. Figure 15 compares the frequency reductions of two longitudinal modes during the test phase for both the AV and WN tests. The evolution of frequency reductions of both modes correlates well with the progression of physical damage of the test building observed at different inspection stages during the test program. Since damage occurred only in the form of local gypsum crushing and incipient screw withdrawal during the serviceability level earthquake test sequence (EQ 1–EQ 4), the frequency reduction remained sufficiently small (5%–10%) for all modes at States S1–S4. The frequency reduction increased substantially at States S6 and S7 due to extensive damage sustained by the structural walls at all but the uppermost levels following the design level (EQ 6) and MCE (EQ 7) tests (see Figure 3A,B). Both longitudinal modes attained frequency reductions of 50%–60% at the end of the pre-fire earthquake test phase (State S7). Despite the fire damage to the gypsum sheathing at Levels 2 and 6 (see Figure 3C,D), no apparent frequency fluctuations occurred following the fire tests (State S8). This is explained by the fact that the earthquake-induced structural damage accumulated during the pre-fire test phase (EQ 1–EQ 7) outweighed the effect

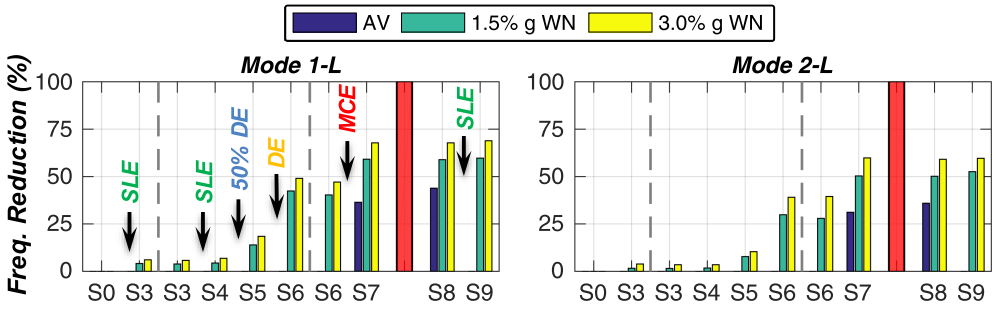

FIGURE 15 Frequency reductions of the of the two longitudinal modes (1-L and 2-L) estimated using the ambient vibration (AV) and white noise (WN) data during the test phase (dashed vertical lines divide earthquake test dates; vertical red bar denotes the fire test phase; DE, design level; MCE, maximum considered earthquake ; SLE, serviceability)

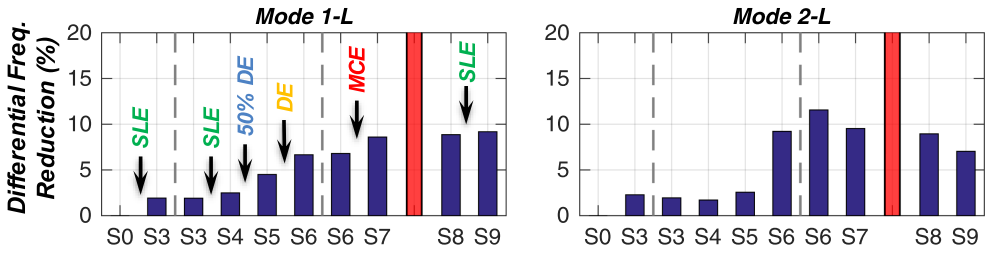

FIGURE 16 Differential frequency reductions of the two longitudinal modes (1-L and 2-L) between the 1.5% *g* and 3.0% *g* WN tests during the test phase (dashed vertical lines divide earthquake test dates; vertical red bar denotes the fire test phase; DE, design level; MCE, maximum considered earthquake level; SLE, serviceability level)

of fire-induced damage (primarily on CFS sheathing). In addition, the post-fire serviceability level test (EQ 8) did not induce further frequency variations of the longitudinal modes due to its low drift demands (PIDR <0.2%).

The frequency evolution of building associated with different vibration excitation sources indicate that these reductions are also dependent on the excitation amplitudes of the vibration tests. Regardless of specific modes, the frequency reduction tends to be higher when obtained from vibration tests with larger excitation amplitudes. Following the end of pre-fire earthquake test phase, for instance, the frequency reductions of both longitudinal modes associated with the 1.5% *g* WN tests were ∼10% lower than those of the 3.0% *g* WN tests during States S7–S9. The reductions obtained from the AV test series were even lower (attaining only 30%–35% for both longitudinal modes) because the acceleration responses during the AV test were about two orders of magnitude smaller than those during the 3.0% *g* WN test (refer to Figure 6). Figure 16 presents the differential frequency reduction of the two longitudinal modes (1-L and 2-L) during the earthquake testing. The differential frequency reduction is defined as the difference between the frequency reductions determined from the 1.5% *g* and 3.0% *g* WN data collected at a specific state, respectively. These results reveal that the differential frequency reduction becomes more substantial in coincidence with the accumulated structural damage. Whereas the differential frequency reductions associated with both longitudinal modes were well below 5% when the building remained essentially linear or quasilinear during the service level and 50% design level tests, namely, States S0–S5. The differences appear noticeably larger following the design level test and reached ∼10% during the last three states, namely, States S7–S9, as the structural damage became more appreciable. This observation indicates that the differential frequency reduction associated with the vibration tests at distinct amplitudes may also serve as an effective metric for structural damage assessment.

6.2 | Story stiffness reduction

Since the interstory drift demands were low during the WN tests, it is assumed that the building response remained linear (or quasilinear) during these low-amplitude vibration tests. Although the lateral force-resisting system of the test building consisted of CFS shear walls, the shear walls were framed as floor-to-floor systems rather than vertically continuous structural elements along the height of the building. Therefore, it is reasonable to characterize the longitudinal building responses in the direction of shaking using simplified shear building models (SBMs), which consist of lumped masses at the floor levels and shear springs to capture the interstory drifts. The equivalent story stiffness of the shear spring is estimated using least-square linear fitting of the shear force versus interstory drift response. In this case, the story shear force of a specific level is calculated as the summation of the inertial forces at floor levels above, while the interstory drift is obtained by double-integrating the absolute floor accelerations at two adjacent floors to obtain the corresponding (absolute) floor displacements and subsequently subtracting these floor displacements to obtain the differential displacements between adjacent floors. The inertial force of a specific floor is determined as the product of the lumped floor mass and absolute floor acceleration. Figure 17 illustrates the measured story shear versus interstory drift response (black) of all levels (Levels 1–6) and the fitted lines (red) during the 1.5% *g* WN test at the reference state (S0). The slope of the fitted line in each plot represents the estimated story stiffness of an individual level. It is observed that while the story stiffness of the upper four levels (1300–1600 kN/cm) remained comparable, they were notably smaller than those of the story stiffness of Levels 1 and 2 (>2200 kN/cm) due to the use of larger diameter steel tie-down rods at the lower two levels.[25] Given the estimated equivalent story stiffness of each level and the mass lumped at each floor,[25] the natural frequencies of the first longitudinal mode (1-L) of the building can also be estimated using the shear

building assumption. Figure 18 compares the natural frequencies of the longitudinal modes ($f_{1\text{-}L}$) estimated using the SBM with those identified directly using the deterministic-stochastic subspace (DSI) identification method from the WN data (refer to Figure 11). This comparison indicates that the first longitudinal mode frequencies derived using the

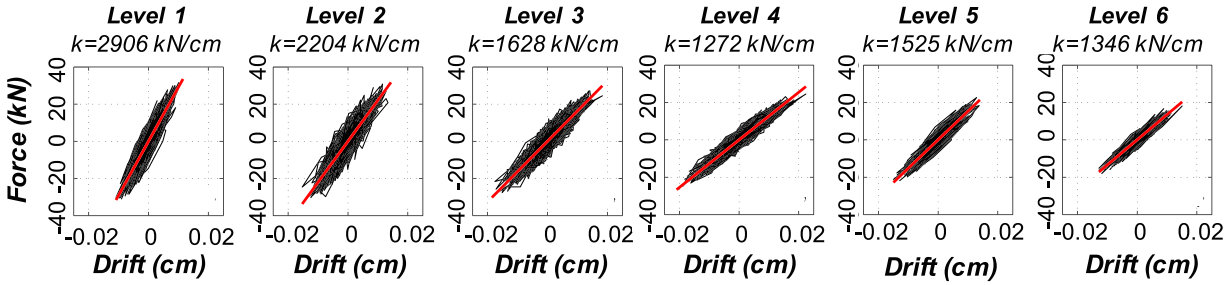

FIGURE 17 Story shear versus interstory drift response during the 1.5% *g* white noise test at the reference state (red lines determined using least-square linear fitting)

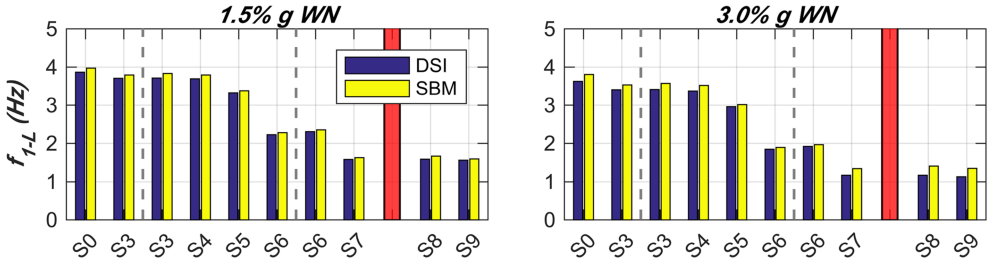

FIGURE 18 Comparison of the frequencies of the first longitudinal mode ($f_{1\text{-}L}$) estimated using the shear building model (SBM) and deterministic-stochastic subspace identification (DSI) method (dashed vertical lines divide earthquake test dates; vertical red bar denotes the fire test phase)

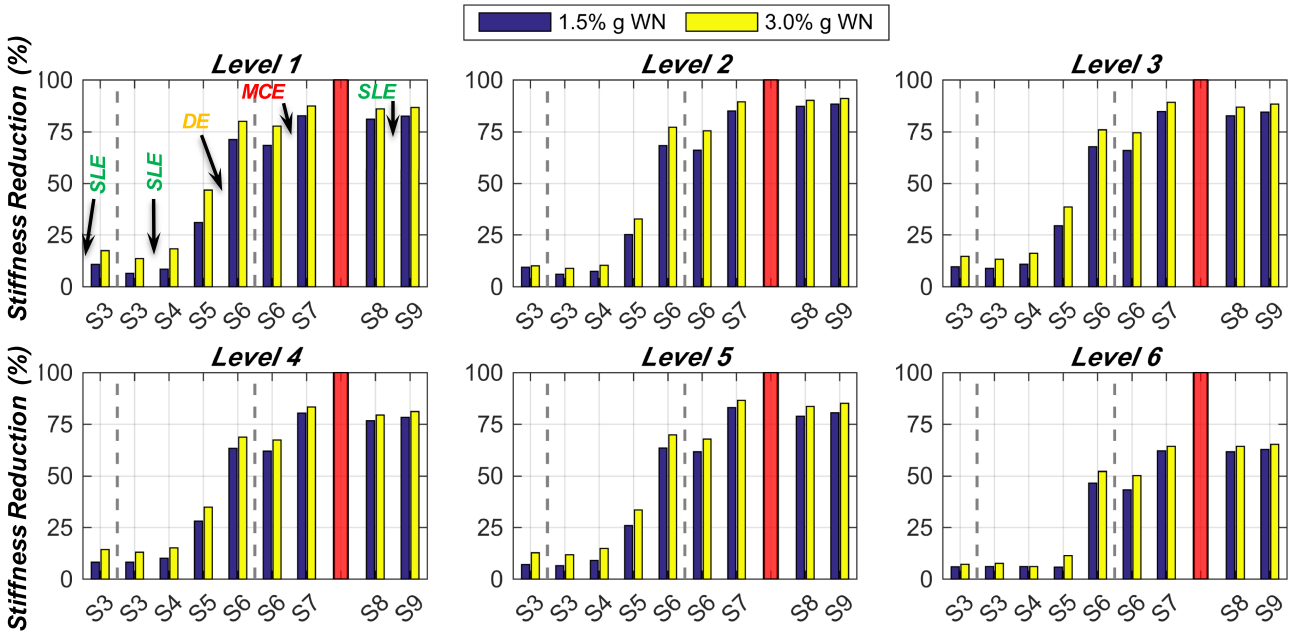

FIGURE 19 Story stiffness reductions of the building estimated using the white noise (WN) data during the test phase (dashed vertical lines divide earthquake test dates; vertical red bar denotes the fire test phase; DE, design level; MCE, maximum considered earthquake ; SLE, serviceability)

SBM agree reasonably well with those identified using the DSI method, since the frequency results obtained from the two methods differ by less than 5%. These comparisons corroborate the validity of the estimated story stiffness and the shear building assumption in reflecting the modal characteristics of the test building.

Figure 19 summarizes the story stiffness reductions of all six levels of the building estimated using the WN data collected during the earthquake test phase. The stiffness reduction (degradation) of a specific story represents a percentage defined as the story stiffness difference between the subsequent state (i.e., S3 through S9) and the reference state (S0) normalized by the story stiffness associated with the reference state. The degradation of the story stiffness correlates well with the evolution of the natural frequencies (see Figure 15). All six levels underwent limited story stiffness reductions (<15%) due to the low seismic drift demands (PIDR <0.1%) during the serviceability level test sequence, that is, States S1–S4. Story stiffness degradation became substantial between States S5 (following 50% design test) and S7 (following MCE test). Following the pre-fire test phase, the story stiffness remained stable for the last three states (S7–S9). Importantly, the story stiffness reduction of Level 6 at both States S6 (following DE test) and S7 (following MCE test) was appreciably smaller than those of the remaining levels (∼60% for Level 6 and >80% for the remaining levels at State S7). The story stiffness reduction distribution is well correlated with the PIDR distribution during the pre-fire tests as well as the observed physical damage. Since the PIDR at Level 6 was less than 0.7% during the pre-fire test phase, damage to the shear walls was essentially in the form of screw withdrawal or minor gypsum crushing, whereas the shear walls at all remaining levels sustained much more extensive wall sheathing damage (Figure 3A–B) due to the higher PIDR demands (1.0%–1.7%). In this regard, the use of the story stiffness reduction as damage metrics provides the potential of localizing structural damage.

7 | CONCLUSIONS

The evolution of modal characteristics of building systems considering a multi-hazard loading scenario consisting of earthquake and ensuing fire events has, to the authors' knowledge, thus far been investigated in only a handful of studies in the literature. This is largely due to the paucity of data available to support such research efforts. In this regard, an experimental program was recently performed to understand the earthquake and post-earthquake fire performance of a mid-rise cold-formed steel (CFS) framed building. In particular, the test building was subjected to a multi-hazard scenario including earthquake, post-earthquake fire, and finally post-fire earthquake loading with companion low-amplitude vibration tests using different sources of excitations, including ambient vibration (AV) and white noise (WN) base excitation tests. These low-amplitude vibration tests were conducted throughout the construction and test phases. The vibration data are used herein to systematically study the evolution of the modal parameters (i.e., natural frequencies, damping ratios, and mode shapes) of the test building at various stages during the multi-hazard test program. The modal parameters are analyzed using four state-of-the-art time-domain system identification (SID) methods, including two input–output (OKID-ERA and DSI) and two output-only (SSI-DATA and NExT-ERA) methods. Regarding the modal characteristics of the CFS test building identified from the low-amplitude vibration test sequence during the construction and test phases, key findings are summarized as follows:

1. Installation of interior gypsum panels on the CFS wall framing and the interior partition wall increased the natural frequencies of the test building by roughly 10% as a result of the stiffness contribution of the gypsum-to-framing fasteners.
2. Comparison of the modal parameters identified from the WN test data at the construction phase demonstrates that the natural frequencies identified using different SID methods are in reasonable agreement with <3% error amongst four different methods, while the identified damping ratios are subjected to much larger method-to-method variability. The discrepancies of estimated damping ratio results reach as much as 30% between the two input–output methods and become even larger between input–output and output-only methods. The presence of large method-to-method variability undermines the validity of adopting damping ratios for quantitative structural damage assessment.
3. The progression of building damage resulted in reduced natural frequencies and increased damping ratios. The frequency reductions remained sufficiently small (<10%) during the serviceability level earthquake test sequence but increased substantially following the design level (as much as 40%) and MCE level tests (exceeded 50%) due to much larger seismic drift demands. However, the fire tests and post-fire serviceability level earthquake test induced no substantial frequency reduction to the earthquake-damaged building. The evolution of the identified modal parameters

correlates well with the progression of physical damage observed during the earthquake-fire test program, demonstrating the effectiveness of the SID methods for structural damage assessment and health monitoring.

4. The natural frequencies and damping ratios are dependent on the amplitudes of the vibration excitations. Increasing the excitation amplitude tends to reduce the natural frequencies but increases the damping ratios. Increasing the RMS amplitude of the WN excitations from 1.5% *g* to 3.0% *g* results in a reduction of the natural frequencies by 10%–15% and an increase of the damping ratios by more than 30%. Furthermore, the frequency reductions are also dependent on the amplitudes of the test excitations. It is therefore important to note that the use of inconsistent excitation amplitudes at different states may result in biased damage assessment observations.
5. Given the story stiffness estimated from the WN tests and the lumped floor mass, the fundamental frequencies of the test building at all damage states derived from the shear beam model agree well with those identified from the SID method. The story stiffness reduction along the height of the building is well correlated with the PIDR distribution at different stages during the pre-fire tests as well as the observed physical damage. In this regard, the use of the story stiffness reduction (degradation) as damage metrics provides the potential to characterize physical damage localization.

ACKNOWLEDGEMENTS

The test program was a collaboration between two academic institutions (University of California, San Diego and Worcester Polytechnic Institute), two government or institutional granting agencies (Department of Housing and Urban Development and the California Seismic Safety Commission), and 15 industry partners. The Jacobs School of Engineering and Department of Structural Engineering at UC San Diego also provided matching support for this effort. It is noted that while UC San Diego led the overall test program with their primary focus was on the earthquake test phases, we are grateful to Prof Brian Meacham and Dr Praveen Kamash from WPI for their leading efforts on the fire testing and contribution to the overall test program. The active collaboration with Prof Gilbert Hegemier from UC San Diego in this test program is also greatly appreciated. In addition, the support of NHERI@UC San Diego staff as well as individuals who contributed greatly to the specimen construction and testing, in particular Tyler Elliot, Srikar Gunissety, Kelly Holcomb, Diego Riveria, and Fernando Sesma, are greatly acknowledged. Opinions and findings of this study are of the authors and do not necessarily reflect those of the sponsors.

ORCID

Xiang Wang https://orcid.org/0000-0002-9845-1875
Tara C. Hutchinson https://orcid.org/0000-0001-9109-7896

REFERENCES

1. Farrar CR, Worden K. An introduction to structural health monitoring. *Philos Trans Royal Soc London A*. 2007;365(1851):303-315.
2. Brownjohn JMW. Structural health monitoring of civil infrastructure. *Philos Trans Royal Soc London A*. 2007;365(1851):589-622.
3. Doebling SW, Farrar CR, Prime MB. A summary review of vibration-based damage identification methods. *Shock Vibr Dig*. 1998;30(2):91-105.
4. Farrar CR, Doebling SW, Nix DA. Vibration–based structural damage identification. *Philos Trans Royal Soc London A*. 2001;359(1778):131-149.
5. Fan W, Qiao PZ. Vibration-based damage identification methods: a review and comparative study. *Struct Health Monit*. 2011;10(5):83-111.
6. Ren WX, De Roeck G. Structural damage identification using modal data. I: simulation verification. *ASCE J Struct Eng*. 2002;128(1):87-95.
7. Johnson E, Lam H, Katafygiotis L, Beck JL. Phase I IASC-ASCE structural health monitoring benchmark problem using simulated data. *ASCE J Eng Mech*. 2004;130(1):3-15.
8. Caicedo JM, Dyke SJ, Johnson EA. Natural excitation technique and eigensystem realization algorithm for phase I of the IASC-ASCE benchmark problem: simulated data. *ASCE J Eng Mech*. 2004;130(1):49-60.
9. Ren WX, De Roeck G. Structural damage identification using modal data. II: test verification. *ASCE J Eng Mech*. 2002;128(1):96-104.
10. Bernal D, Dyke SJ, Lam HF, Beck JL. Phase II of the ASCE benchmark study on SHM. *Proc., 15th ASCE Engineering Mechanics Conference*, New york, NY, 2002.
11. Giraldo D, Song W, Dyke S, Caicedo J. Modal identification through ambient vibration: comparative study. *ASCE J Eng Mech*. 2009;135(8):759-770.
12. Brownjohn JMW. Ambient vibration studies for system identification of tall buildings. *Earthq Eng Struct Dyn*. 2003;32(1):71-95.
13. Farrar C, James IG. System identification from ambient vibration measurements on a bridge. *J Sound Vib*. 1997;205(1):1-18.

14. Peeters B, De Roeck G. One-year monitoring of the Z24-bridge: environmental effects versus damage events. *Earthq Eng Struct Dyn*. 2001;30(2):149-171.
15. He X, Moaveni B, Conte JP, Elgamal A, Masri SF. System identification of Alfred Zampa memorial bridge using dynamic field test data. *ASCE J Struct Eng*. 2009;135(1):54-66.
16. Çelebi M, Ulusoy HS, Nakata N. Responses of a tall building in Los Angeles, California, as inferred from local and distant earthquakes. *Earthq Spectra*. 2016;32(3):1821-1843.
17. Ventura CE, Schuster ND. Structural dynamic properties of a reinforced concrete high-rise building during construction. *Can J Civ Eng*. 1996;23(4):950-972.
18. Yousefianmoghadam S, Behmanesh I, Stavridis A, Moaveni B, Nozari A, Sacco A. System identification and modeling of a dynamically tested and gradually damaged 10-story reinforced concrete building. *Earthq Eng Struct Dyn*. 2018;47(1):25-47.
19. Moaveni B, He X, Conte JP, Restrepo JI, Panagiotou M. System identification study of a 7-story full-scale building slice tested on the UCSD-NEES shake table. *ASCE J Struct Eng*. 2010;137(6):705-717.
20. Ji X, Fenves G, Kajiwara K, Nakashima M. Seismic damage detection of a full-scale shaking table test structure. *ASCE J Struct Eng*. 2011;137(1):14-21.
21. Belleri A, Moaveni B, Restrepo JI. Damage assessment through structural identification of a three-story large-scale precast concrete structure. *Earthq Eng Struct Dyn*. 2014;43(1):61-76.
22. Wang X, Astroza R, Hutchinson TC, Conte JP, Restrepo JI. Dynamic characteristics and seismic behavior of prefabricated steel stairs in a full-scale five-story building shake table test program. *Earthq Eng Struct Dyn*. 2015;44(14):2507-2527.
23. Astroza R, Ebrahimian H, Conte JP, Restrepo JI, Hutchinson TC. System identification of a full-scale five-story reinforced concrete building tested on the NEES-UCSD shake table. *Struct Control Health Monit*. 2016;23(3):535-559.
24. Wang X, Hutchinson TC, Hegemier G, Gunisetty S, Kamath P, Meacham B. Earthquake and post- earthquake fire performance of a mid-rise cold-formed steel framed building—test program and test results: rapid release report (CFS Test Program Report #1). *Structural Systems Research Project. Report No. SSRP-16/07*. University of California, San Diego, La Jolla, CA, USA, 2016.
25. Wang X, Hutchinson TC, Hegemier G, Gunisetty S, Kamath P, Meacham B. Earthquake and post- earthquake fire performance of a mid-rise cold-formed steel framed building–test program and test results: Final report (CFS Test Program Report #2). *Structural Systems Research Project. Report No. SSRP-16/08.* University of California, San Diego, La Jolla, CA, USA, 2018.
26. Hutchinson TC, Wang X, Hegemier G, Meacham B, Kamath P, Sesma F, Holcome K. Earthquake and post-earthquake fire performance of a mid-rise cold-formed steel framed building. *Proc., 2017 SEAOC convention,* San Diego, CA, USA, 2017.
27. Schafer BW. Cold-formed steel structures around the world: a review of recent advances in applications, analysis and design. *Steel Construct*. 2011;4(3):141-149.
28. AISI (American Iron and Steel Institute). *North American standard for cold-formed steel farming—lateral design*. Washington, DC: AISI S213; 2007.
29. AISI (American Iron and Steel Institute). *North American specification for the design of cold-formed steel structural members*. Washington DC: AISI S100; 2012.
30. ASCE (American Society of Civil Engineers). *Minimum Design Loads for Buildings and Other Structures*. Reston, VA: ASCE 7; 2010.
31. Welch P. The use of fast Fourier transform for the estimation of power spectra: a method based on time averaging over short, modified periodograms. *IEEE Trans Audio Electroacoust*. 1967;15(2):70-73.
32. Van Overschee P, De Moor B. *Subspace Identification for Linear Systems: Theory-Implementation-Applications*. Norwell, MA: Kluwer Academic Publishers; 1996.
33. Juang JN, Pappa RS. An Eigensystem realization algorithm for modal parameter identification and model reduction. *J Guid Control Dynam*. 1985;8(5):620-627.
34. Juang JN, Phan M, Horta LG, Longman RW. Identification of observer/Kalman filter Markov parameters: theory and experiments. *J Guid Control Dynam*. 1993;16(2):320-329.
35. Peeters B, De Roeck G. Stochastic system identification for operational modal analysis: a review. *J Dyn Syst Measure Control*. 2001;123 (4):659-667.
36. James GH, Carne TG, Lauffer JP. The natural excitation technique (NExT) for modal parameter extraction from operating structures. *Int J Anal Exper Modal Anal*. 1995;10(4):260-277.
37. Heylen W, Sas P. *Modal analysis theory and testing*. Katholieke Universteit Leuven: Departement Werktuigkunde; 2006.
38. Allemang RJ, Brown DL. A correlation coefficient for modal vector analysis. *Proc. 1st International Modal Analysis Conference*, Bethel, CT, USA, 1982.

How to cite this article: Wang X, Hutchinson TC. Evolution of modal characteristics of a mid-rise cold-formed steel building during construction and earthquake testing. *Earthquake Engng Struct Dyn*. 2020;49:1539–1558. https://doi.org/10.1002/eqe.3316